The intestinal metal transporter ZIP14 maintains systemic manganese homeostasis

Received for publication, April 5, 2019, and in revised form, April 24, 2019 Published, Papers in Press, April 26, 2019, DOI 10.1074/jbc.RA119.008762

Ivo Florin Scheiber, Yuze Wu, Shannon Elizabeth Morgan, and Ningning Zhao[1]

From the Department of Nutritional Sciences, University of Arizona, Tucson, Arizona 85721

Edited by Ruma Banerjee

ZIP14 (encoded by the solute carrier 39 family member 14 (*SLC39A14*) gene) is a manganese transporter that is abundantly expressed in the liver and small intestine. Loss-of-function mutations in *SLC39A14* cause severe hypermanganesemia. Because the liver is regarded as the main regulatory organ involved in manganese homeostasis, impaired hepatic manganese uptake for subsequent biliary excretion has been proposed as the underlying disease mechanism. However, liver-specific *Zip14* KO mice exhibit decreased manganese only in the liver and do not develop manganese accumulation in other tissues under normal conditions. This suggests that impaired hepatobiliary excretion is not the primary cause for manganese overload observed in individuals lacking functional ZIP14. We therefore hypothesized that increased intestinal manganese absorption could induce manganese hyperaccumulation when ZIP14 is inactivated. To elucidate the role of ZIP14 in manganese absorption, here we used CaCo-2 Transwell cultures as a model system for intestinal epithelia. The generation of a ZIP14-deficient CaCo-2 cell line enabled the identification of ZIP14 as the major transporter mediating basolateral manganese uptake in enterocytes. Lack of ZIP14 severely impaired basolateral-to-apical (secretory) manganese transport and strongly enhanced manganese transport in the apical-to-basolateral (absorptive) direction. Mechanistic studies provided evidence that ZIP14 restricts manganese transport in the absorptive direction via direct basolateral reuptake of freshly absorbed manganese. In support of such function of intestinal ZIP14 *in vivo*, manganese levels in the livers and brains of intestine-specific *Zip14* KO mice were significantly elevated. Our findings highlight the importance of intestinal ZIP14 in regulating systemic manganese homeostasis.

Manganese is an essential nutrient. As a cofactor for several enzymes, it is required for the normal function of several physiologic processes including protein glycosylation, detoxification of superoxide and ammonia, and gluconeogenesis (1, 2). Excessive manganese accumulation, however, leads to manganism, whose symptoms resemble those of Parkinson's disease (1). Therefore, manganese homeostasis must be tightly controlled at the systemic and cellular levels.

Systemic manganese homeostasis is maintained by intestinal manganese absorption and hepatobiliary manganese excretion (3–6). Oral exposure is the major source of manganese absorption with ~2–3% of manganese being absorbed from a diet adequate in manganese (7). For dietary manganese intakes that are in the physiologic range, oral manganese absorption appears to be primarily controlled by varying intestinal absorption rates (8). However, biliary manganese elimination becomes the main homeostatic mechanism when intestinal control mechanisms are overwhelmed or bypassed, *e.g.* by intravenous injection or inhalation exposure.

On a cellular level, the distribution of manganese involves mechanisms for entry and exit, as well as specific pathways that ensure intracellular transport and targeting. To date, these mechanisms remain poorly defined. Components of the iron metabolic pathways; citrate, choline, dopamine, and calcium transporters; the sodium-calcium exchanger; as well as the ATPases Park9 and SPCA1 have been implicated in manganese metabolism (9). More recently, spurred by the discovery of human mutations, members of the ZnT and ZIP families of metal transporters, namely ZnT10, ZIP8, and ZIP14, have been identified as crucial players in cellular manganese metabolism *in vivo* (10–14).

Previous studies have shown that ZIP14 is capable of mediating the uptake of manganese *in vitro* (15). Highlighting the function of ZIP14 as a manganese transporter *in vivo*, homozygous mutations of *ZIP14* result in manganese hyperaccumulation in the blood and other tissues of affected individuals without apparent effects on other metals (10, 16–18). Initially it was postulated that the primary function of ZIP14 is hepatic manganese uptake for subsequent biliary excretion and that the manganese hyperaccumulation observed in other tissues is secondary to the defect of hepatic ZIP14 (10). The latter hypothesis, however, was falsified by experiments involving a liver-specific *Zip14* KO mouse line (19). Specifically, these mice did not display elevated manganese in the blood or other tissues in contrast to global *Zip14* KO mouse models, although ZIP14 has been clearly demonstrated to be required for hepatobiliary manganese excretion under high manganese conditions (19–22).

ZIP14 is also highly abundant in the small intestines of humans and mice (23, 24). We hypothesize that, if not impaired hepatobiliary excretion, increased intestinal man-

This work was supported by National Institutes of Health Grant R00DK104066 (to N. Z.). The authors declare that they have no conflicts of interest with the contents of this article. The content is solely the responsibility of the authors and does not necessarily represent the official views of the National Institutes of Health.

This article contains Figs. S1–S8.

[1] To whom correspondence should be addressed: Dept. of Nutritional Sciences, University of Arizona, Tucson, AZ 85721. Tel.: 520-621-9744; Fax: 520-621-9446; Email: zhaonn@email.arizona.edu.

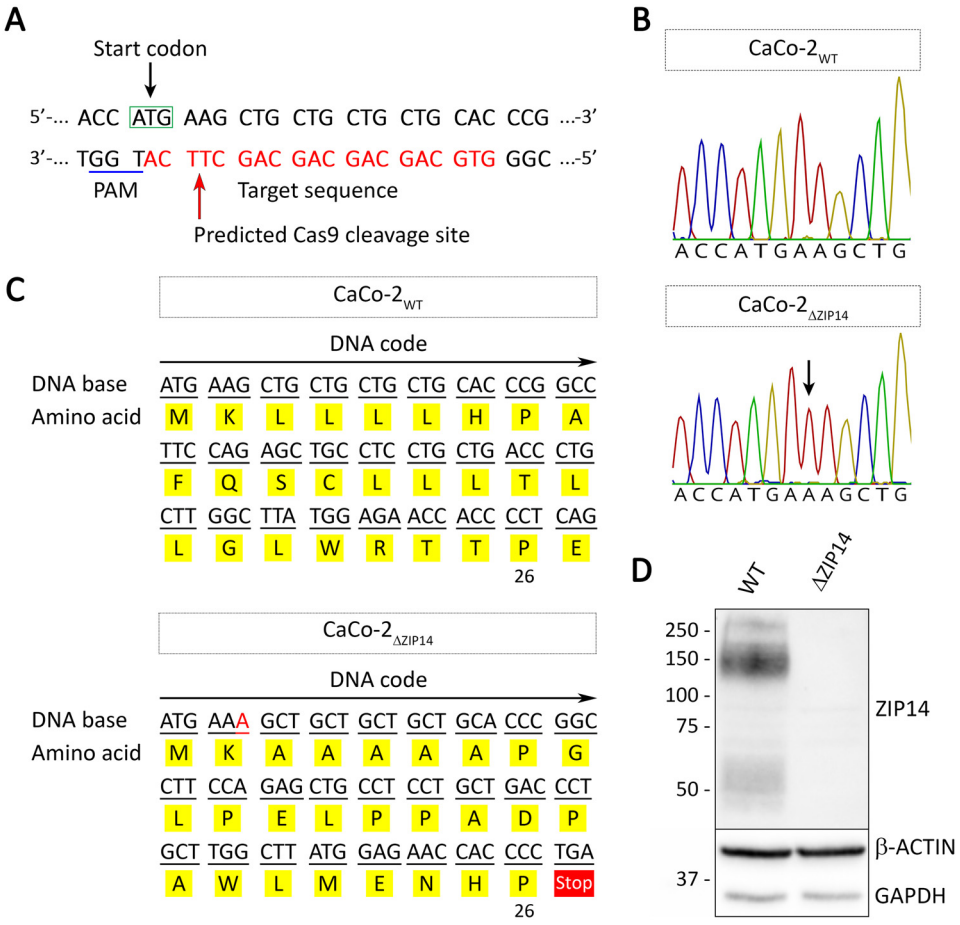

Figure 1. Generation of a *ZIP14* KO CaCo-2 cell line (CaCo-$2_{\Delta ZIP14}$). *A*, schematic illustration of CRISPR/Cas9-mediated genome editing to generate CaCo-$2_{\Delta ZIP14}$ cells. The DNA sequence covering the start codon of *ZIP14* within exon 2 is shown. The guide RNA sequence is marked in *red letters*, and the PAM (protospacer adjacent motif) sequence is *underlined* in *blue*. The *red arrow* marks the predicted Cas9 cleavage site. *B*, chromatograms of sequencing results using DNA isolated from CaCo-2_{WT} and CaCo-$2_{\Delta ZIP14}$ cells. The *black arrow* indicates the insertion of an adenosine at the predicted Cas9 cleavage site. *C*, the single adenosine insertion results in a frameshift with premature translation termination after amino acid 26. *D*, ZIP14 immunoblot of whole-cell lysates of CaCo-2_{WT} (*WT*) and CaCo-$2_{\Delta ZIP14}$ (Δ*ZIP14*) cells confirms the deletion of ZIP14 in CaCo-$2_{\Delta ZIP14}$ cells. Both β-ACTIN and GAPDH were used as loading controls.

ganese absorption could be the primary cause for the manganese hyperaccumulation observed in individuals lacking functional ZIP14. To test our hypothesis, we generated a CaCo-2 cell line with *ZIP14* inactivation (CaCo-$2_{\Delta ZIP14}$ cells). Differentiated monolayers of this cell line exhibited a dramatic defect in basolateral manganese uptake. Apical-to-basolateral manganese transport in CaCo-$2_{\Delta ZIP14}$ cells was strongly increased compared with that of WT CaCo-2 (CaCo-2_{WT}) cells. Further mechanistic studies provided evidence that ZIP14 controls enterocyte manganese absorption by mediating basolateral reuptake of freshly absorbed manganese. To evaluate the physiologic relevance of this novel homeostatic mechanism, we generated intestine-specific *Zip14* KO mice. These mice developed markedly increased manganese levels in their livers and brains. Overall, our results suggest an important function of intestinal ZIP14 in the control of systemic manganese homeostasis.

Results

Generation of a ZIP14 KO CaCo-2 cell line

To assess the function of ZIP14 in enterocytes, we inactivated the *ZIP14* gene in CaCo-2 cells via CRISPR/Cas9-mediated[2] gene KO by targeting the start codon in exon 2 of *ZIP14* (Fig. 1*A*). CaCo-2 cells differentiate spontaneously into polarized enterocytes when grown on permeable filter supports (25). Such CaCo-2 cell cultures provide a well-established model system to study the uptake as well as absorptive (apical-to-basolateral direction) and secretory (basolateral-to-apical direction) fluxes of drugs and nutrients in the intestinal epithelium. This model has been extensively used to study the mechanisms of intestinal iron uptake and transport. In general, results from iron absorption studies conducted *in vitro* using CaCo-2 cells correlate well with observations made *in vivo* (26), validating the use of the CaCo-2 cell model for studying intestinal metal uptake and transport.

By using the CRISPR/Cas9 approach, we isolated a CaCo-2 cell clone termed CaCo-$2_{\Delta ZIP14}$ with a single-base pair inser-

[2] The abbreviations used are: CRISPR, clustered regularly interspaced short palindromic repeat; ANOVA, analysis of variance; DAPI, 4′,6-diamidino-2-phenylindole; DFO, desferrioxamine; DMEM, Dulbecco's modified Eagle's medium; DMT1, divalent metal transporter 1; GAPDH, glyceraldehyde 3-phosphate dehydrogenase; GST, glutathione *S*-transferase; HRP, horseradish peroxidase; ICP-MS, inductively coupled plasma mass spectrometry; LY, Lucifer yellow; TBS, Tris-buffered saline; ZnT, zinc transporter; ZO-1, zonula occludens-1.

tion at the predicted Cas9-cleavage site (Fig. 1*B*). This insertion caused a frameshift mutation, yielding a nonfunctional protein that consists of only 26 amino acids (Fig. 1*C*). Immunoblot analysis confirmed the inactivation of *ZIP14* in CaCo-$2_{\Delta ZIP14}$ cells (Fig. 1*D* and Fig. S1).

Characterization of CaCo-2_{WT} and CaCo-$2_{\Delta ZIP14}$ Transwell cultures

To study manganese transport across the intestinal epithelium and the role of ZIP14 in this process, both CaCo-2_{WT} and CaCo-$2_{\Delta ZIP14}$ cells were grown into differentiated monolayers for at least 21 days. The presence of polarized monolayers was confirmed by confocal microscopy using the tight junction protein ZO-1 as the apical marker and Na^+,K^+-ATPase as the basolateral marker (Fig. 2*A*). Further analysis of these images revealed diameters of 11 and 9 μm and heights of 12 and 19 μm for CaCo-2_{WT} cells and CaCo-$2_{\Delta ZIP14}$ cells, respectively. The consequential larger basolateral and apical surface areas and volumes of CaCo-$2_{\Delta ZIP14}$ Transwell cultures, which we estimated to be ~180 and 150% of equivalent CaCo-2_{WT} cultures, are mirrored by a similar increase in the protein contents of these cultures (Fig. 2*B*). Thus, to compensate for the increased surface, we normalized our uptake and transport data to the protein content in the respective Transwell insert. The integrity of the monolayers was tested by the Lucifer yellow (LY) rejection assay. Apparent LY permeability (P_{app}) coefficients below 10 nm $\times$ s^{-1} have been reported to be indicative of well-established CaCo-2 monolayers (27). P_{app} coefficients determined for both CaCo-2_{WT} and CaCo-$2_{\Delta ZIP14}$ monolayers fell in that range but were significantly higher in CaCo-$2_{\Delta ZIP14}$ Transwell cultures (Fig. 2*C*). Because of the smaller diameter of CaCo-$2_{\Delta ZIP14}$ cells, CaCo-$2_{\Delta ZIP14}$ Transwell cultures possess a greater number of paracellular pores, the sites of paracellular transport, which may partially account for the increased permeability of LY. Consequently, when normalized to protein, P_{app} did not differ significantly between the cultures.

Deletion of *Zip14* in mice does not affect the intestinal contents of manganese, zinc, iron, and copper (19). To test whether this observation is reflected in the CaCo-2 Transwell system, we measured their specific contents by inductively coupled plasma MS (ICP-MS). We found the specific contents of manganese, zinc, and iron in CaCo-$2_{\Delta ZIP14}$ monolayers to be significantly lower compared with those in CaCo-2_{WT} cells (Fig. 2*D*). We ascribe this discrepancy to the *in vivo* situation to limitations of our Transwell system. *In vivo* enterocytes can acquire nutrients from both the intestinal lumen and the arterial blood. Transporters functioning in metal uptake from the luminal side of the proximal intestine, such as DMT1, are optimally adjusted to the acidic milieu of the intestinal tract (28–30). In the Transwell system, however, the pH in the apical chamber is maintained at 7.4 during regular culturing, impairing efficient metal uptake from this side.

To confirm previous results on the localization of ZIP14 in enterocytes (21, 31) we studied the localization of ZIP14 in polarized CaCo-2_{WT} monolayers. Basolateral and apical surface proteins were isolated by a biotinylation approach. Immunoblotting for ZIP14 demonstrated the enrichment of ZIP14 at the basolateral membrane of CaCo-2_{WT} cells (Fig. 2*E* and Fig. S2). This localization of ZIP14 in enterocytes supports a role of ZIP14 in the uptake of manganese from the blood.

ZIP14 is the major transporter responsible for manganese uptake at the basolateral membrane

To establish the function of ZIP14 in the manganese metabolism of enterocytes, we first studied the consequences of *ZIP14* KO on basolateral ^{54}Mn accumulation. If not stated otherwise, during the experiments the extracellular pH was maintained at 6.1 in the apical and 7.4 in the basolateral compartment to mimic the physiologic situation, *i.e.* the acidic intraluminal pH of the proximal small intestine and the normal blood pH. Upon addition of 0.1 μM ^{54}Mn, which is close to the low manganese concentrations in mammalian serum (0.01–0.04 μM; Ref. 32) to the basolateral chamber, CaCo-2_{WT} cells rapidly accumulated ^{54}Mn up to 180 min, after which cellular ^{54}Mn contents had reached a steady state (Fig. 3*A*). Basolateral ^{54}Mn accumulation by CaCo-$2_{\Delta ZIP14}$ cells was severely compromised, identifying ZIP14 as the primary transporter mediating manganese uptake at the basolateral membrane of CaCo-2 cells. The residual basolateral ^{54}Mn accumulation observed in CaCo-$2_{\Delta ZIP14}$ cells suggests the presence of an alternative, low-capacity entry route for manganese at the basolateral membrane.

Next we examined the pH dependence of basolateral manganese accumulation by measuring the amount of ^{54}Mn accumulated by CaCo-2 cells incubated in media at pH 6.1, pH 6.8, or pH 7.4 for 4 h. These experiments were performed by adjusting the incubation media to the same pH in both the basolateral and apical compartments. Basolateral ^{54}Mn accumulation by CaCo-2_{WT} cells was maximal at pH 7.4 and decreased with decreasing pH (Fig. 3*B*). Although CaCo-2_{WT} cells still accumulated substantial amounts of ^{54}Mn at pH 6.8, the basolateral ^{54}Mn accumulation in these cells decreased by ~90% at pH 6.1. Consistent with ZIP14 being the major transporter mediating manganese uptake at the basolateral membrane of CaCo-2_{WT} cells, similar pH dependences have been reported for ZIP14-mediated iron and zinc transport (33, 34). Opposite to what we observed for CaCo-2_{WT} cells, basolateral ^{54}Mn accumulation by CaCo-$2_{\Delta ZIP14}$ cells was maximal at pH 6.1 and lower at pH 6.8 and 7.4.

ZIP14 deletion does not substantially affect apical manganese uptake

In contrast to the striking effect of *ZIP14* KO observed for basolateral ^{54}Mn accumulation, ^{54}Mn accumulation from the apical chamber was observed to be rather similar in both cell lines. Within 6 h both CaCo-2_{WT} and CaCo-$2_{\Delta ZIP14}$ cells accumulated ~30 pmol $\times$ mg^{-1} ^{54}Mn from the apical chamber (Fig. 3*C*). Although apical ^{54}Mn accumulation by CaCo-$2_{\Delta ZIP14}$ cells proceeded at slightly faster pace between 30 min and 3 h of incubation, ^{54}Mn contents in CaCo-$2_{\Delta ZIP14}$ cells approached a steady state thereafter, whereas ^{54}Mn contents in CaCo-2_{WT} cells continued to rise at almost constant speed for up to 6 h. Manganese accumulation by CaCo-2 cells is a complex process involving the uptake and export of manganese at the apical side, its intracellular sequestration and transport, and its basolateral uptake and export. The accelerated accumulation of ^{54}Mn from

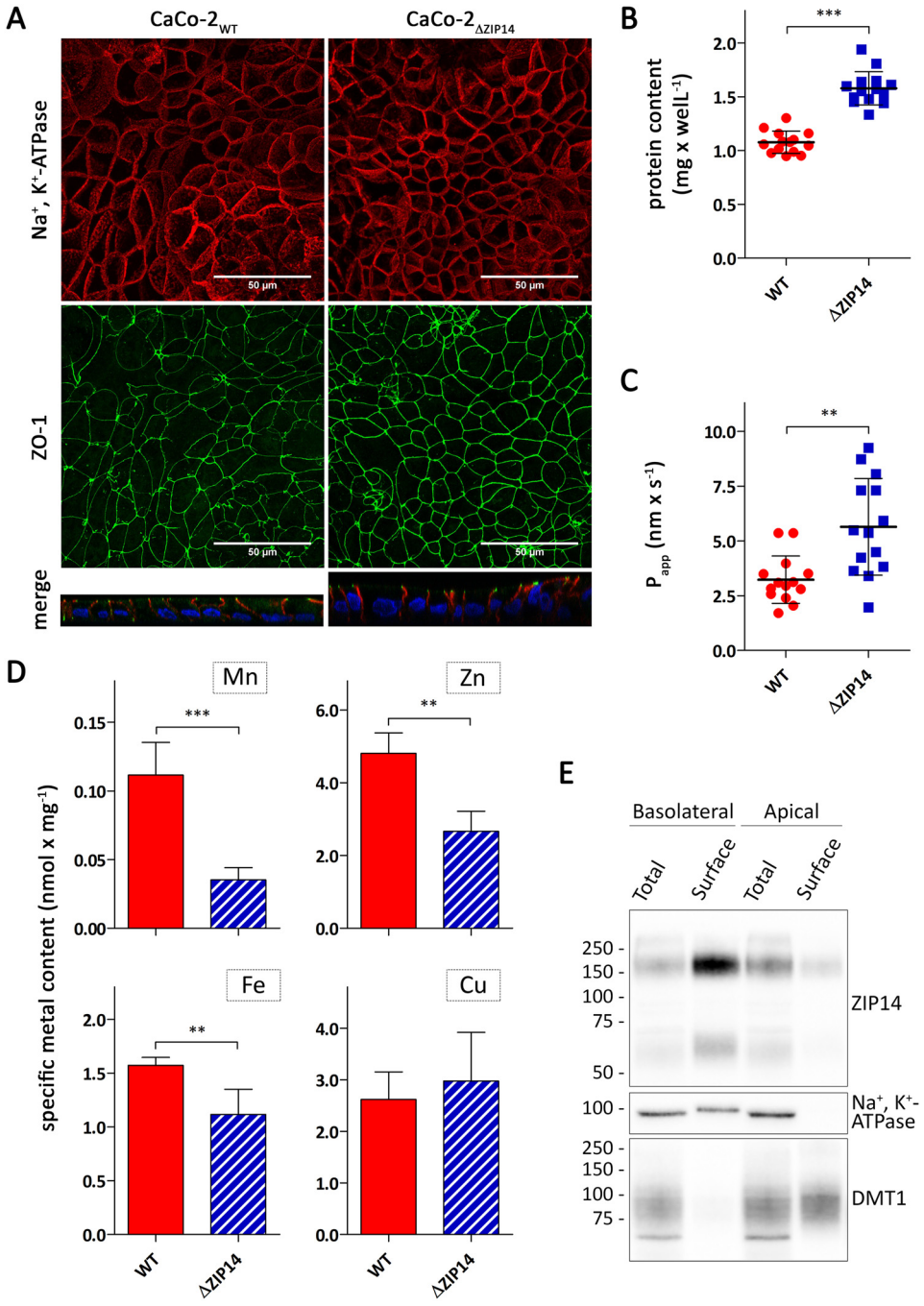

Figure 2. Characterization of CaCo-2$_{WT}$ and CaCo-2$_{\Delta ZIP14}$ Transwell cultures. *A*, confocal microscopy of CaCo-2$_{WT}$ and CaCo-2$_{\Delta ZIP14}$ cells co-immunostained for Na^+,K^+-ATPase and ZO-1. The nuclei were stained with 4′,6-diamidino-2-phenylindole dihydrochloride. The *four upper panels* show the orthogonal maximum projections of 42- and 69-frame stacks for CaCo-2$_{WT}$ and CaCo-2$_{\Delta ZIP14}$ cells, respectively. The *two bottom panels* show a perpendicular projection of merged Na^+,K^+-ATPase (*red*) and ZO-1 (*green*) proteins with nuclei (*blue*). The *scale bars* (50 μm) in the *upper panels* also apply to the *bottom panels*. *B–D*, total protein content (*B*), apparent permeability (P_{app}) of Lucifer yellow (*C*), and specific contents of manganese, zinc, iron, and copper of CaCo-2$_{WT}$ (*WT*) and CaCo-2$_{\Delta ZIP14}$ (Δ*ZIP14*) Transwell cultures (*D*). The data are presented as means ± S.D. from 13 (*B* and *C*) or 3 (*D*) independent prepared cultures. Statistical analysis was performed using Student's *t* test. **, $p < 0.01$; ***, $p < 0.001$. *E*, CaCo-2$_{WT}$ Transwell cultures were subjected to basolateral or apical surface biotinylation with cell membrane-impermeable Sulfo-NHS-SS-biotin. Biotin-labeled cell-surface proteins (*Surface*) were isolated from whole-cell lysates (*Total*) using NeutrAvidin-agarose beads. 45 μg of whole-cell lysates (*Total*) and 15 μg of biotin-labeled cell-surface proteins (*Surface*) were analyzed by immunoblotting for ZIP14. Na^+,K^+-ATPase served as the basolateral marker and DMT1 as the apical marker.

the apical side by CaCo-2$_{\Delta ZIP14}$ cells compared with CaCo-2$_{WT}$ cells between 30 min and 3 h may therefore be explained by several mechanisms, including a ZIP14-dependent export process of freshly acquired manganese (either at the basolateral or apical side) that is activated when cellular manganese levels rise above a certain threshold.

Apical ^{54}Mn accumulation exhibited the same dependence on the extracellular pH in both CaCo-2$_{WT}$ and CaCo-2$_{\Delta ZIP14}$ cells, being maximal at pH 6.1 and decreasing with increasing pH (Fig. 3*D*). Although this is relevant under physiological conditions, because the pH in the proximal intestine is rather acidic, the mechanisms mediating manganese uptake from the

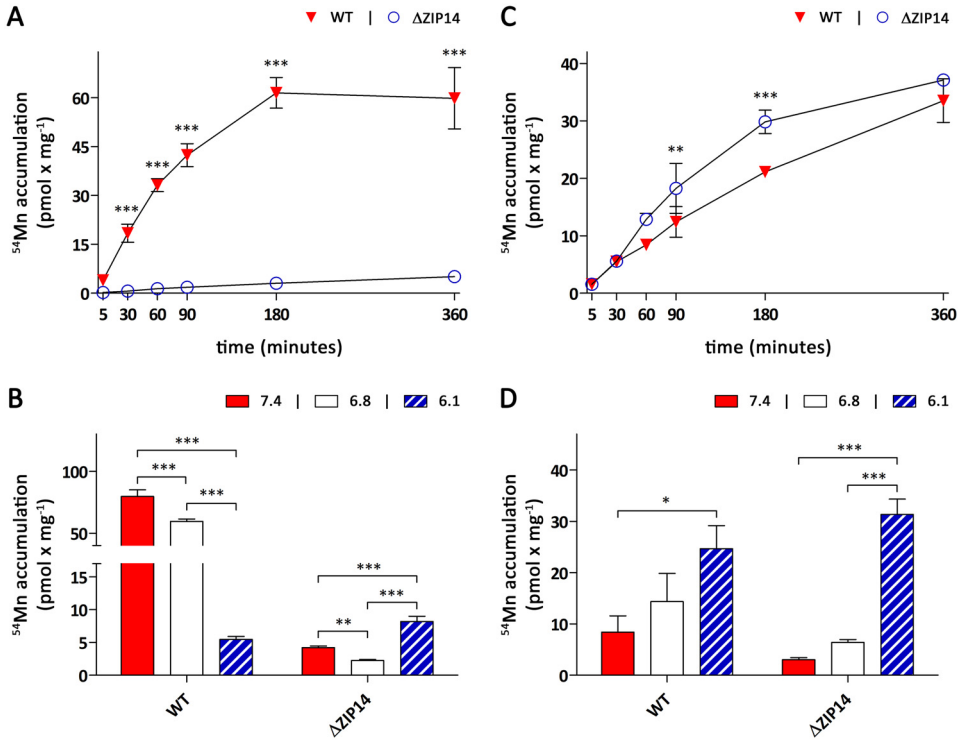

Figure 3. Manganese uptake by CaCo-2_{WT} and CaCo-$2_{\Delta ZIP14}$ monolayers. Uptake experiments were initiated by adding manganese citrate spiked with ^{54}Mn either to the basolateral (*A* and *B*) or apical compartment (*C* and *D*). *A* and *C*, time dependence of manganese uptake by CaCo-2_{WT} (*WT*) and CaCo-$2_{\Delta ZIP14}$ (*ΔZIP14*) cells in the presence of 0.1 μM ^{54}Mn citrate. During the uptake experiments the extracellular pH was maintained at pH 7.4 in the basolateral and pH 6.1 in the apical compartment. *B* and *D*, pH dependence of manganese uptake by WT and ΔZIP14 cells. The cells were incubated for 4 h in the presence of 0.1 μM ^{54}Mn citrate. During the experiments, the pH levels of both the apical and basolateral compartment were maintained at the pH indicated in the figures. The data are presented as means ± S.D. from three independent experiments performed in duplicate. Statistical analysis was performed using two-way ANOVA followed by the Bonferroni post hoc test. *, $p < 0.05$; **, $p < 0.01$; ***, $p < 0.001$.

intestinal lumen remain unknown. DMT-1, which is strongly expressed at the intestinal brush border (35) and at the apical membrane of CaCo-2 cells (Fig. 2*E*), had long been regarded as a potential candidate. However, recently Shawki *et al.* (36) reported that DMT-1 is not required for manganese absorption in intestine-specific *Dmt-1* KO mice, contrasting previous observations made in the Belgrade rat model (37, 38).

ZIP14 restricts manganese absorption

Having established that ZIP14 is the major transporter mediating basolateral manganese uptake and that ZIP14 deletion does not substantially affect manganese uptake from the apical membrane of CaCo-2 cells, we next investigated the transport of manganese across CaCo-2 cell monolayers in both basolateral-to-apical and apical-to-basolateral directions. Upon application of 0.1 μM ^{54}Mn to the basolateral side of CaCo-2_{WT} cells, the amounts of ^{54}Mn detected in the apical chamber rapidly increased with time (Fig. 4*A*). Following an exponential phase that lasted ~90 min, the amounts of ^{54}Mn on the apical side increased almost linearly for up to 240 min. In contrast, CaCo-$2_{\Delta ZIP14}$ cells transported only minimal amounts of ^{54}Mn from the basolateral to apical compartment within 240 min. This result could be expected because CaCo-$2_{\Delta ZIP14}$ cells lack substantial basolateral manganese uptake activity.

After addition of 0.1 μM ^{54}Mn to the apical chamber to initiate the apical-to-basolateral transport, we observed a slow, exponential rise in the amounts of ^{54}Mn detected in the apical chamber in the first 150 min followed by a linear increase for up to 240 min for CaCo-2_{WT} cells (Fig. 4*B*). The time dependence of apical-to-basolateral manganese transport by CaCo-$2_{\Delta ZIP14}$ cells displayed a similar pattern but with significantly higher amounts of ^{54}Mn accumulated in the basolateral compartment. The increased apical-to-basolateral manganese transport by CaCo-$2_{\Delta ZIP14}$ cells compared with CaCo2_{WT} cells strongly suggests that intestinal ZIP14 is required to restrict manganese absorption.

ZIP14 has been described as a broad-scope metal transporter, capable of mediating the cellular uptake of several metals including iron (33, 34). Hence, we tested the consequences of ZIP14 deletion on iron accumulation and transport in CaCo-2 cell monolayers upon addition of 1 μM $^{59}Fe^{2+}$ or $^{59}Fe^{3+}$. Consistent with the function of ZIP14 as a Fe^{2+} transporter, basolateral $^{59}Fe^{2+}$ accumulation was lowered by 30% in CaCo-$2_{\Delta ZIP14}$ cells, whereas $^{59}Fe^{3+}$ accumulation did not differ significantly from CaCo-2_{WT} cells (Fig. S3*A*). In contrast to manganese transport, the lack of ZIP14 did not affect the apical-to-basolateral transport of $^{59}Fe^{2+}$ or $^{59}Fe^{3+}$ (Fig. S3, *C* and *D*), most likely because iron is released from the cells into the media in its ferric state. This result suggests that in the CaCo-2 Transwell system, functional ZIP14 specifically restricts manganese absorption.

ZIP14 mediates manganese reuptake from the basolateral membrane to restrict manganese absorption

In CaCo-2 cells, ZIP14 restricts the flux of manganese in the absorptive direction (Fig. 4*B*), but how is it accomplished?

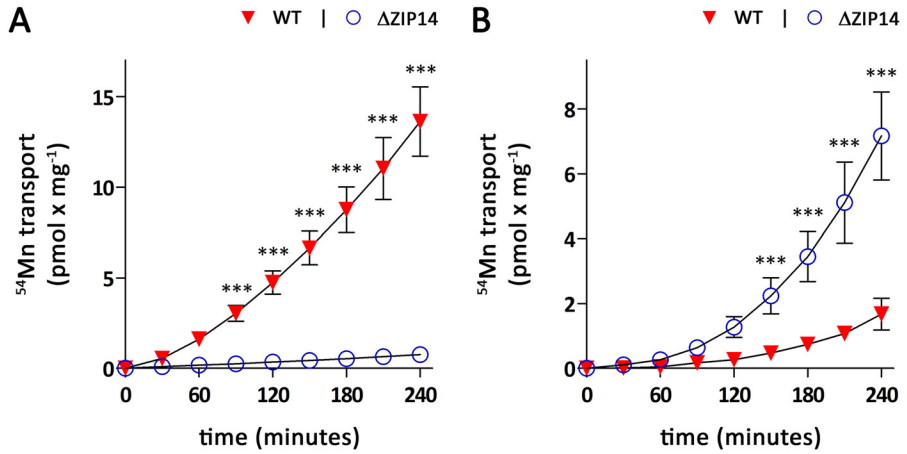

Figure 4. Manganese transport by CaCo-2_{WT} and CaCo-$2_{\Delta ZIP14}$ monolayers. Manganese transport experiments were initiated by adding 0.1 μM ^{54}Mn citrate either to the basolateral (*A*) or apical (*B*) compartment of CaCo-2_{WT} (*WT*) and CaCo-$2_{\Delta ZIP14}$ (Δ*ZIP14*) monolayers. Samples were collected every 30 min from the opposite compartment and analyzed by γ-counting. During the transport experiments, the extracellular pH was maintained at pH 7.4 in the basolateral and pH 6.1 in the apical compartment. The data are presented as means ± S.D. from three independent experiments performed in duplicate. Statistical analysis was performed using two-way ANOVA followed by the Bonferroni post hoc test. ***, $p < 0.001$.

ZIP14 is localized to the basolateral membrane of CaCo-2 cells (Fig. 2*E*) and is required for efficient manganese uptake from the basolateral side (Fig. 3, *A* and *B*). Accordingly, direct reuptake of freshly absorbed manganese is a plausible mechanism by which ZIP14 may restrict manganese absorption. If so, inhibiting basolateral manganese uptake should increase apical-to-basolateral manganese transport in CaCo-2_{WT} cells, but not in CaCo-$2_{\Delta ZIP14}$ cells. We used three approaches to minimize basolateral manganese reuptake.

First, because ZIP14-mediated ^{54}Mn uptake is highest at pH 7.4 and decreases by 95% at pH 6.1 (Fig. 3*B*), we studied the transport of 0.1 μM ^{54}Mn from the apical to basolateral compartment with the pH in the basolateral chamber being maintained at pH 7.4 as the normal condition or adjusted to pH 6.1. For CaCo-2_{WT} cells, ^{54}Mn accumulation in the basolateral chamber was found to be approximately five times higher at a basolateral pH of 6.1 compared with a basolateral pH of 7.4 (Fig. 5*A*). In contrast, apical-to-basolateral manganese transport by CaCo-$2_{\Delta ZIP14}$ cells slightly decreased with lowering the basolateral pH from pH 7.4 to pH 6.1 (Fig. 5*B*). These observations are consistent with the pH dependence of basolateral manganese accumulation (Fig. 3*B*) and suggest that manganese transport in the apical-to-basolateral direction is limited by basolateral manganese uptake.

Apical-to-basolateral manganese transport requires ~150 min to become fully established (Fig. 4*B*). To exclude that the modulation of basolateral mediated manganese uptake by altering the basolateral pH induces changes in the recruitment of transporters required for the export of intracellular manganese at the basolateral side, we removed ^{54}Mn from the apical compartment after 4 h of ^{54}Mn preloading and followed ^{54}Mn accumulation in the basolateral compartment for another 3 h, with the pH of the basolateral compartment either maintained at the same pH as in the first 4 h or switched to pH 6.1 or pH 7.4 (Fig. 5, *C–F*). Alteration of the basolateral pH caused a rapid response in the apical-to-basolateral transport rates. The immediate effect of the basolateral pH switch on the apical-to-basolateral manganese transport in CaCo-2 cells suggests that the elevated manganese absorption at lower pH observed in CaCo-2_{WT} cells is indeed due to impaired ZIP14 mediated manganese uptake at low pH rather than due to alterations in transporter abundance at the basolateral membrane.

Second, we used excess zinc to compete with ^{54}Mn reuptake from the basolateral chamber. Zinc has previously been reported as a potent competitive inhibitor of ZIP14-mediated manganese uptake (33). However, initial experiments revealed that a 10-fold excess of zinc does not inhibit basolateral ^{54}Mn accumulation by CaCo-2_{WT} cells when Dulbecco's modified Eagle's medium (DMEM) was used as the experimental medium (Fig. S4*A*). In contrast, when salt-based incubation buffer was used instead of DMEM, excess zinc strongly impaired basolateral ^{54}Mn accumulation in CaCo-2_{WT} cells (Fig. S4*B*). Thus, to study the effect of zinc on apical-to-basolateral transport, CaCo-2 monolayers were first loaded for 4 h with 0.1 μM ^{54}Mn from the apical side, after which the accumulation of ^{54}Mn in the basolateral compartment was followed for 90 min using salt-based incubation buffer with or without 2 μM zinc. The presence of 2 μM zinc strongly enhanced ^{54}Mn accumulation in the basolateral compartment of CaCo-2_{WT} Transwell cultures (Fig. 6*A*), suggesting that zinc impairs the direct reuptake of freshly absorbed manganese by competing with ^{54}Mn for uptake via ZIP14. Consistent with this view, ^{54}Mn accumulation in the basolateral compartment of CaCo-$2_{\Delta ZIP14}$ Transwell cultures (Fig. 6*B*) was not altered by zinc.

Third, we sought to prevent ZIP14-mediated manganese reuptake by chelating freshly absorbed manganese with EDTA or desferrioxamine (DFO), which are strong chelators for Mn(II) and Mn(III), respectively (39, 40). Because both EDTA and DFO are membrane-impermeable (41), the intracellular manganese trafficking would not be disturbed. To carry out the experiment, CaCo-2 monolayers were first loaded for 4 h with 0.1 μM ^{54}Mn from the apical side, after which the accumulation of ^{54}Mn in the basolateral compartment was followed for 90 min using salt-based incubation buffer containing either no chelator, 100 μM $CaNa_2EDTA$, or 1 mM DFO. The presence of both EDTA or DFO caused an increased accumulation of ^{54}Mn

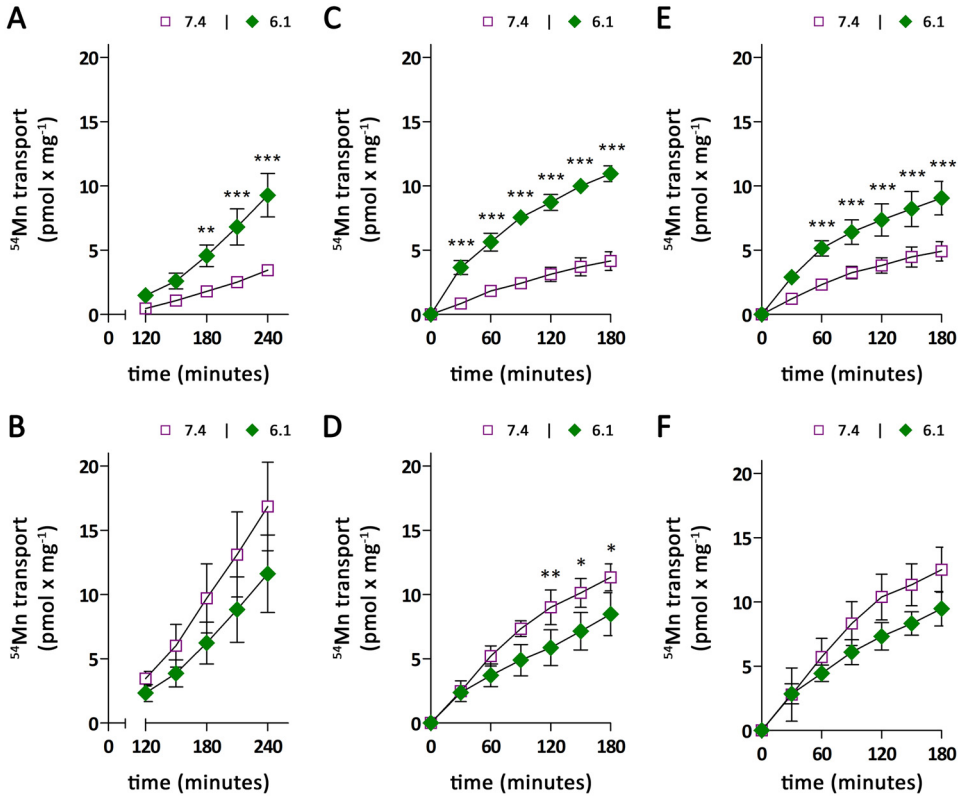

Figure 5. Modulation of apical to basolateral manganese transport by extracellular pH. Manganese-transport experiments were initiated by adding 0.1 μM ^{54}Mn citrate to the apical compartment of CaCo-2$_{WT}$ (*A*, *C*, and *E*) and CaCo-2$_{\Delta ZIP14}$ (*B*, *D*, and *F*) monolayers. Throughout the transport experiments, the extracellular pH in the apical compartment was maintained at pH 6.1. *A* and *B*, the cells were incubated for 240 min maintaining the basolateral pH at either pH 7.4 or pH 6.1. Samples were collected between 120 and 240 min for γ-counting. *C–F*, the cells were loaded for 240 min with 0.1 μM ^{54}Mn citrate from the apical side with the basolateral pH maintained at pH 7.4 (*C* and *D*) or pH 6.1 (*E* and *F*). Subsequently ^{54}Mn was removed, the cells were washed thrice with PBS$^{Ca/Mg}$ from both sides and transferred to fresh 6-well plates. The accumulation of ^{54}Mn in the basolateral compartment was followed for another 180 min, with the pH of the basolateral compartment either maintained at pH 7.4 or at pH 6.1. The data are presented as means ± S.D. from three independent experiments. Statistical analysis was performed using two-way ANOVA followed by the Bonferroni post hoc test. *, $p < 0.05$; **, $p < 0.01$; ***, $p < 0.001$.

in the basolateral compartment of CaCo-2$_{WT}$ Transwell cultures (Fig. 6, *C* and *E*) but not in CaCo-2$_{\Delta ZIP14}$ Transwell cultures (Fig. 6, *D* and *F*). Because manganese is released close to the plasma membrane, the moderate effect of both chelators on the accumulation of ^{54}Mn in the basolateral compartment of CaCo-2$_{WT}$ Transwell cultures is most likely due to limited access of EDTA and DFO to manganese prior to its reuptake. Nevertheless, these results further support our proposed mechanism that ZIP14 restricts manganese absorption by direct reuptake of freshly absorbed manganese.

Intestine-specific deletion of Zip14 in mice leads to manganese overload

To test the physiologic relevance of our findings, we generated mice carrying *Zip14* conditional alleles (*Zip14*$^{flox/flox}$ mice) by flanking exons 3 and 4 of the *Zip14* with *loxP* sites (Fig. 7*A*). The correct insertion of *loxP* sites was verified by genotyping (Fig. 7*B*). We then generated intestine-specific *Zip14* KO mice by crossing *Zip14*$^{flox/flox}$ mice with *Vil-Cre* mice. For comparison, we also generated liver-specific *Zip14* KO mice. Tissue-specific inactivation of *Zip14* was confirmed by immunoblot analysis (Fig. 7*C* and Fig. S5).

We used ICP-MS to determine manganese levels in whole blood, livers, and brains from *Zip14*$^{flox/flox}$ mice, intestine-specific, and liver-specific *Zip14* KO mice at 3 weeks of age. We observed a clear difference in the hepatic manganese levels from liver-specific *Zip14* KO mice and intestine-specific *Zip14* KO mice (Fig. 7*D*): consistent with previous results (19), hepatic manganese contents were significantly reduced in liver-specific *Zip14* KO mice; in contrast, manganese levels in livers from intestine-specific *Zip14* KO mice were more than two times that of controls, revealing that loss of ZIP14 in the intestine increases body manganese burden. This observation establishes the importance of the intestinal ZIP14 in the control of systemic manganese homeostasis and is in full agreement with our discovery that deletion of ZIP14 in CaCo-2 cells results in increased apical-to-basolateral manganese transport.

Although manganese concentrations in the blood of intestine-specific *Zip14* KO mice did not increase (Fig. 7*D*), brain manganese contents were double that of control and liver-specific *Zip14* KO mice at 3 weeks old. An explanation could be that manganese homeostasis can still be regulated through hepatobiliary excretion in intestine-specific *Zip14* KO mice, but the liver cannot clear all of the excess manganese entering the portal blood, and elevated manganese entering the systemic circulation is readily absorbed by other tissues, including the brain. Further studies are required to evaluate the manganese contents in other tissues of intestine-specific *Zip14* KO mice

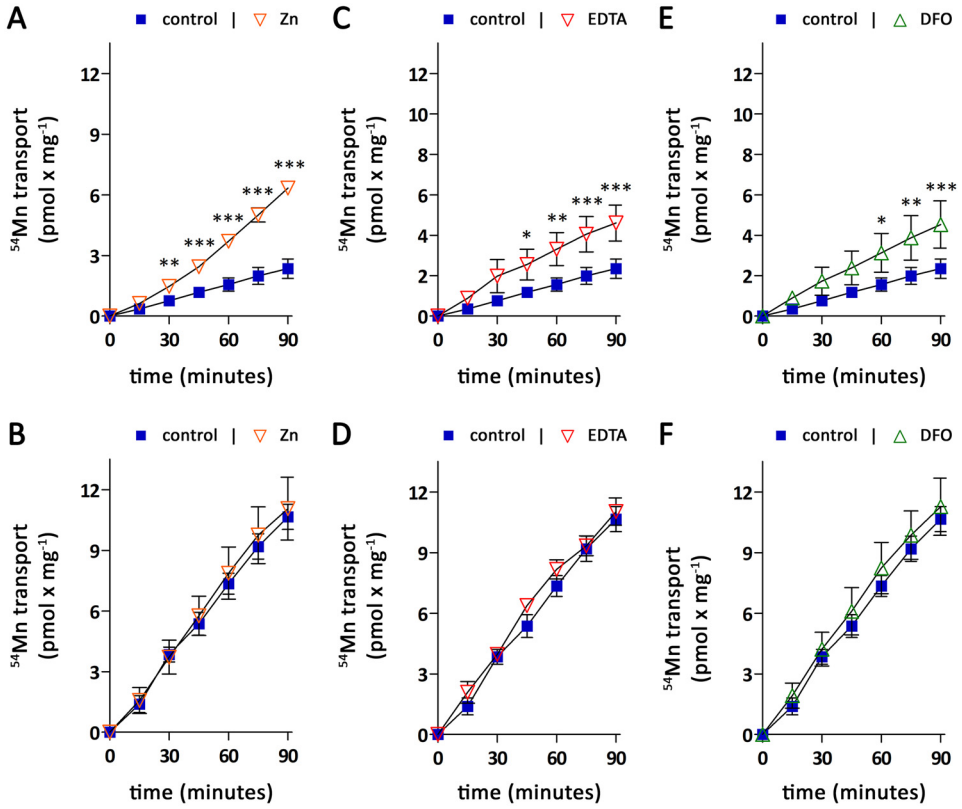

Figure 6. Modulation of apical to basolateral manganese transport by zinc competition or chelators. Manganese-transport experiments were initiated by adding 0.1 μM ^{54}Mn citrate to the apical compartment of CaCo-2$_{WT}$ (*A*, *C*, and *E*) and CaCo-2$_{\Delta ZIP14}$ (*B*, *D*, and *F*) monolayers. Throughout the transport experiments, the extracellular pH in the apical compartment was maintained at pH 6.1. The cells were loaded for 240 min with 0.1 μM ^{54}Mn citrate from the apical side with the basolateral pH maintained at pH 7.4. Subsequently ^{54}Mn was removed, the cells were washed thrice with PBS$^{Ca/Mg}$ from both sides and transferred to fresh 6-well plates. The basolateral medium was changed from DMEM to salt-based incubation buffer adjusted to pH 7.4 (control) containing 2 μM $ZnCl_2$ (*A* and *B*), 100 μM $CaNa_2EDTA$ (*C* and *D*), or 1 mM DFO (*E* and *F*), and the accumulation of ^{54}Mn in the basolateral compartment was followed for another 90 min. The data are presented as means ± S.D. from three independent experiments. Statistical analysis was performed using two-way ANOVA followed by the Bonferroni post hoc test. *, $p < 0.05$; **, $p < 0.01$; ***, $p < 0.001$.

and to examine the consequences of *Zip14* deletion in both the liver and intestine.

Discussion

In the present study, we identified ZIP14 as the major transporter mediating basolateral manganese uptake in enterocytes. Moreover, we provide *in vitro* and *in vivo* evidence that this function of ZIP14 is required for the control of manganese homeostasis.

CaCo-2 cell cultures provide a well-established model system to study the uptake and the absorptive and secretory fluxes of drugs and nutrients in the intestinal epithelium (25). Genetically modified CaCo-2 cell lines have previously been used to study the uptake and transport of metals. Just recently, a stable CaCo-2 cell line overexpressing ZnT10 has been employed to prove the ability of this transporter to mediate the efflux of cellular manganese at the apical membrane (52). RNAi-mediated gene knockdown has been used to study the functions of ZnT1, ferroportin, and DMT1 in CaCo-2 cell monolayers (42, 43). A drawback of RNAi-mediated gene knockdown is the possibility of residual gene expression that may mask potential phenotypes, a complication that we avoided by generating a *ZIP14* KO CaCo-2 cell line using the CRISPR/Cas9 system.

In contrast to previous studies investigating manganese uptake and manganese transport by CaCo-2 cells (44–46), we maintained a pH of 6.1 in the apical and a pH of 7.4 in the basolateral compartment to mimic the physiologic situation. Such pH gradient is routinely used in studies investigating iron uptake and iron transport in CaCo-2 cells and is of the uttermost importance when studying apical manganese uptake and apical-to-basolateral manganese transport because substantial manganese transport in the absorptive direction occurs only at acidic apical pH (Fig. S6). To account for the low manganese concentrations in mammalian serum (0.01–0.04 μM; Ref. 32), breast milk (0.004–0.55 μM; Ref. 47), and infant formulas (0.73–20 μM; Ref. 48), we used a concentration of 0.1 μM manganese as our standard concentration, whereas nonphysiologic high manganese concentrations of 30–146 μM were employed in the previous studies (44–46).

Systemic manganese homeostasis is maintained by the regulation of both intestinal manganese absorption and hepatobiliary manganese excretion (3–6). The accumulation of excess manganese in blood and several organs in individuals with homozygous mutations in *ZIP14* (10, 16–18) and global *Zip14* KO mice (19–22) indicates a crucial requirement of ZIP14 in systemic manganese homeostasis. ZIP14 has convincingly been shown to mediate hepatobiliary manganese excretion in concert with ZnT10 (20). However, in contrast to the global *Zip14* KO mice, liver-specific *Zip14* KO mice do not hyperaccumu-

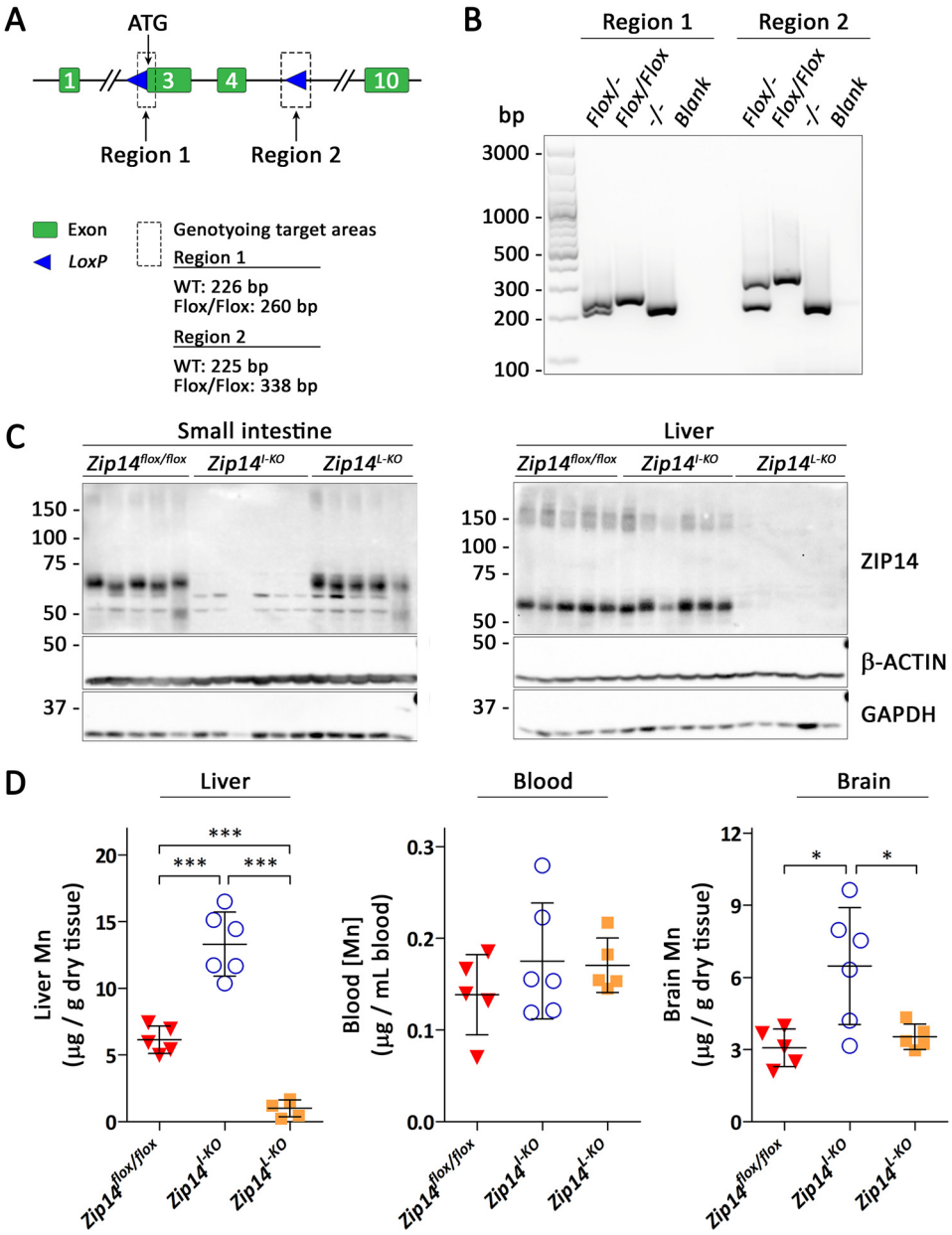

Figure 7. Intestine-specific deletion of *Zip14* in mice leads to manganese overload. *A*, gene targeting strategy for generating mice carrying *Zip14* conditional alleles. *B*, genotyping results using DNA isolated from heterozygous (Flox/−), homozygous (Flox/Flox), and WT (−/−) mice. *C*, ZIP14 immunoblot of small intestine and liver samples from $Zip14^{flox/flox}$ ($n = 5$, 3 male and 2 female), intestine-specific ($Zip14^{I\text{-}KO}$, $n = 6$, 3 male and 3 female), and liver-specific (*Zip14*L-KO, $n = 5$, 3 male and 2 female) *Zip14* KO mice. Both β-ACTIN and GAPDH were used as loading controls. *D*, levels of manganese in livers, blood, and brains of 3-week-old $Zip14^{flox/flox}$, $Zip14^{I\text{-}KO}$, and *Zip14*L-KO mice. Statistical analysis was performed using one-way ANOVA followed by the Bonferroni post hoc test. *, $p < 0.05$; ***, $p < 0.001$.

late manganese (19), indicating that ZIP14 is involved in extrahepatic processes required for the maintenance of systemic manganese homeostasis.

In the present study, we identified ZIP14 as the primary transporter mediating efficient manganese uptake from the basolateral side of enterocytes. This function of ZIP14 is consistent with its localization in the intestine and CaCo-2 monolayers (21, 31) and the reported pH dependences of ZIP14-mediated iron and zinc uptake (33, 34). Our results also indicate that CaCo-2 cells possess alternative systems to acquire manganese from the basolateral compartment that become evident in $CaCo2_{\Delta ZIP14}$ cultures; however, because of the low capacity, these mechanisms are unlikely to compensate for the loss of ZIP14 function *in vivo*.

Apical manganese uptake does not differ substantially in $CaCo\text{-}2_{WT}$ and $CaCo2_{\Delta ZIP14}$ cultures, but *ZIP14* inactivation strongly enhances the flux of manganese in the absorptive direction, suggesting that functional ZIP14 is required to limit manganese absorption. Mechanistically, we demonstrate that inhibiting ZIP14-mediated basolateral manganese uptake by lowering the basolateral pH, zinc competition, and chelation of freshly absorbed manganese all increase manganese transport in the absorptive direction. These observations strongly support that intestinal ZIP14 contributes to the maintenance of

systemic manganese homeostasis by restricting dietary manganese absorption via direct reuptake of freshly absorbed manganese. Such function of intestinal ZIP14 would not only explain the manganese hyperaccumulation observed in individuals lacking functional ZIP14 but also the lack of manganese accumulation in the liver-specific *Zip14* KO mice.

Providing evidence that ZIP14 restricts dietary manganese absorption *in vivo*, intestine-specific *Zip14* KO mice display elevated manganese contents in the liver and brain, indicating that enterocyte-specific KO of *Zip14* causes manganese overload. However, these mice do not develop increased blood manganese concentrations at 3 weeks of age because the liver control system is still in place and excess manganese is likely to be cleared from the blood by extrahepatic tissues, including the brain.

In summary, we show that ZIP14 is crucial for efficient manganese uptake from the basolateral membrane of enterocytes. We provide evidence that one potential mechanism by which ZIP14 restricts manganese absorption and limits whole body manganese burden is through direct reuptake of freshly absorbed manganese. Moreover, our *in vivo* data provide strong evidence that intestinal ZIP14 plays an important role in maintaining systemic manganese homeostasis.

Experimental procedures

Cell cultures

CaCo-2 (ATCC HTB-37^{TM}) cells were maintained in growth medium (80% DMEM containing 1 mM pyruvate; Corning, Corning, NY) supplemented with 3.7 g $\times$ liter^{-1} $NaHCO_3$, 1$\times$ nonessential amino acids (Thermo Fisher Scientific), 100 units $\times$ ml^{-1} penicillin, 100 μg $\times$ ml^{-1} streptomycin (Thermo Fisher Scientific), and 20% fetal bovine serum (VWR, Radnor, PA) at 37 °C and 5% CO_2 in the humidified atmosphere of an incubator. The manganese concentration of the growth medium was determined to be 0.056 $\pm$ 0.005 μM by ICP-MS as described under "ICP-MS analysis of metals" (Fig. S7). The cells were split every 3–4 days following detachment by treatment with 0.25% trypsin in PBS without calcium and magnesium and containing 0.2% EDTA (Thermo Fisher Scientific). For routine cell culture, the cells were seeded in cell culture dishes of 55 cm^2 (Thermo Fisher Scientific) at a density of 0.1 $\times$ 10^4 (CaCo-2$_{WT}$) or 0.14 $\times$ 10^4 (CaCo2$_{\Delta ZIP14}$) cells per cm^2. For preparation of CaCo-2 cell monolayers, 1 $\times$ 10^5 cells/cm^2 were seeded in Transwell-Clear^{TM} inserts with 0.4-μm pore size of 4.67 or 1.12 cm^2 surface area (both from Corning) that had been incubated with growth medium for 24 h prior to seeding. Inserts of 4.67 (1.12) cm^2 were placed in 6-well (12-well) plates with 2.6 (1.5) ml of growth medium in the well and 1.5 (0.5) ml in the insert. The growth medium was changed every 2–3 days. CaCo-2 cell monolayers were used for experiments between 21 and 27 days after seeding.

Generation of a CaCo-2 ZIP14 KO cell line

The CaCo-2 *ZIP14* KO cell line was generated using the CRISPR-Cas9 system (49). The guide RNA sequence (5′-GTG CAG CAG CAG CAG CTT CA-3′), complementary to a sequence in proximity to the start codon of the *ZIP14* gene, was cloned into the pX330-U6-Chimeric_BB-CBh-hSpCas9 vector (50). CaCo-2 cells were transfected with *ZIP14*-targeting vector using Lipofectamine^{TM} 3000 (Thermo Fisher Scientific). Briefly, on the day of the transfection, CaCo-2 cells were seeded in 12-well plates (Thermo Fisher Scientific) at a density of 0.2 $\times$ 10^4 cell/cm^2 and incubated for 6 h in growth medium without penicillin and streptomycin. The medium was changed to growth medium, and the DNA–lipid complex (1 μg of plasmid DNA, 2 μl of P3000^{TM} reagent, 3 μl of Lipofectamine^{TM} 3000 reagent, 95 μl of DMEM), prepared 3 h in advance according to the protocol provided by the manufacturer, was added dropwise to the cells. The cells were grown for 72 h, after which the medium was changed to growth medium containing 7.5 μg $\times$ ml^{-1} puromycine for selection. After 48 h the cells contained in one well were split into four culture dishes of 55 cm^2 and cultured for 3 weeks in growth medium. Single-cell clones were transferred to 12-well plates for screening by immunoblot analysis with a human ZIP14-specific antibody described under "Antibodies." Cell clones lacking ZIP14 expression were subcloned. *ZIP14* inactivation in selected subclones was confirmed by immunoblot analysis and DNA sequencing.

Animals

All mice were maintained on a NIH-31 irradiated traditional rodent diet (Teklad 7913; Envigo, Indianapolis, IN) and housed in the laboratory animal facility at the University of Arizona. Procedures for animal experiments were approved by the institutional animal care and use committee. Mice carrying *Zip14* conditional alleles (*Zip14*$^{flox/flox}$ mice) were generated by flanking exons 3 and 4 of *Zip14* gene with *loxP* sites (Cyagen, Santa Clara, CA). The transgenic mice expressing Cre recombinase under the intestine-specific villin promotor (*Vil-Cre* mice) and liver-specific albumin promoter (*Alb-Cre* mice) were purchased from the Jackson Laboratory. All mice are on the C57BL/6 background. Genotyping procedures were performed by using mouse tail snipping and the Mouse Direct PCR kit (Bimake, Houston, TX). The mice were sacrificed after anesthetizing with ketamine/xylazine at 3 weeks of age. Tissues were collected and immediately frozen in liquid nitrogen and stored at −80 °C until further analyses.

Antibodies

Because antibodies against mouse ZIP14 (mZIP14) and human ZIP14 (hZIP14) are not commercially available, we employed the approach of expressing glutathione *S*-transferase (GST) fusion proteins in *Escherichia coli* to produce and purify the immunogens for the production of antibodies. To construct a vector carrying mZIP14 or hZIP14 fusion protein, the sequence encoding N-terminal serine 31 to proline 146 of mZIP14 or serine 32 to proline 148 of hZIP14 was PCR-amplified and cloned into pGEX-3X (Addgene, Watertown, MA) vector using BamHI–EcoRI linkers. The fusion protein was isolated from *E. coli* and purified by affinity chromatography on gluthathione–Sepharose 4B (GE Healthcare). The immunization procedures were performed by the Pocono Rabbit Farm & Laboratory (Canadensis, PA). The antisera obtained from the test bleeds were analyzed for ZIP14 recognition by immunoblotting. Antisera were cleared by GSH–Sepharose cross-linked with GST to remove anti-GST antibody. The cleared

flow-through fractions were collected and used to purify anti-hZIP14 or anti-mZIP14 antibody using GSH–Sepharose cross-linked with GST-mZIP14 or GST-hZIP14 fusion protein (Fig. S8).

The rabbit anti–ZO-1 polyclonal antibody (21773-1-AP), rabbit anti-DMT1 polyclonal antibody (20507-1-AP), horseradish peroxidase (HRP)-conjugated mouse anti-β-actin mAb (HRP-60008), HRP-conjugated mouse anti-GAPDH mAb (HRP-60004), and HRP-conjugated goat anti mouse IgG (H+L) secondary antibody (SA00001-1) were from Proteintech (Rosemont, IL). The monoclonal mouse anti-Na^+,K^+-ATPase α1 antibody (sc-21712) was from Santa Cruz (Dallas, TX). HRP-conjugated goat anti-rabbit IgG (H+L) secondary antibody (65-6120), Alexa Fluor 594-conjugated donkey anti-mouse IgG (H+L) secondary antibody (A21203), and Alexa Fluor 488-conjugated goat anti-rabbit (A21206) secondary antibody were from Thermo Fisher Scientific.

Immunoblot analysis

Cells and mouse tissues were lysed in NETT buffer (150 mM NaCl, 5 mM EDTA, 10 mM Tris, 1% Triton X-100, and 1× protease inhibitor mixture (Bimake, Houston, TX), pH 7.4). The nuclei were removed by centrifugation (15,000 × *g* at 4 °C for 15 min). Protein concentrations of cell lysates were determined using the RC DC™ protein assay (Bio-Rad). Cell lysates were mixed with 1× Laemmli buffer and incubated for 30 min at 37 °C. The proteins were separated electrophoretically on an SDS/10% polyacrylamide gel and transferred to nitrocellulose membranes (GVS, Sanford, ME). Following blocking of unspecific binding sites with 5% (w/v) nonfat dry milk in TBS with Tween 20 (TBS-T; 10 mM Tris/HCl, 150 mM NaCl, 0.1% (v/v), 1 ml of Tween 20, pH 7.5), membranes were probed at 4 °C overnight with rabbit anti-hZIP14 (1:3000), anti-mZIP14, or anti-DMT1 (1:5000) antibodies in blocking buffer. The membranes were washed four times with TBS-T (5 min each) and subsequently incubated for 1 h at room temperature with HRP-conjugated goat anti-rabbit secondary antibodies (1:5000). After two washes with TBS-T and TBS (5 min each), the blots were developed using enhanced chemiluminescence (SuperSignal West Pico, Thermo Fisher Scientific) and the ChemiDoc™ MP Imaging System (Bio-Rad). To confirm equivalent loading, blots were stripped for 15 min in Restore PLUS Western blotting stripping buffer (Thermo Fisher Scientific), blocked for 1 h in blocking buffer, and reprobed with HRP-conjugated antibodies directed against GAPDH (1:20,000) and/or β-ACTIN (1:20,000). Mouse anti-Na^+,K^+-ATPase (1:3000) followed by HRP-conjugated secondary antibodies (1:5000) served as loading control for plasma membrane proteins. The blots were visualized and quantified using the ChemiDoc MP imaging system with Image Lab software (Bio-Rad).

Isolation of genomic DNA, PCR, and sequencing

Genomic DNA was isolated using the Quick-DNA™ Miniprep Plus Kit (Zymo Research, Irvine, CA) according to the protocol provided by the manufacturer. The guide RNA targeting region in exon 2 of the *ZIP14* gene was amplified with DNA-specific primers (forward primer, 5′-GAG CAG AGA AGC AGA GAC TGA-3′; reverse primer, 5′-ACG GTA AGG CTC CCC TGT-3′). PCR products were isolated by agarose gel electrophoresis and purified with the Wizard SV Gel and PCR Clean-Up System (Promega Corporation, Madison, WI). The purified PCR products were sent for sequencing to MCLAB (San Francisco, CA).

ICP-MS analysis of metals

CaCo-2 cell monolayers grown on Transwell inserts were washed twice with PBS, after which membranes were excised with a scalpel, transferred to 1.5-ml reaction tubes, and frozen in liquid nitrogen. The cells were lysed by repeated freeze-thaw in 1 ml of MilliQ-water, and an aliquot of 25 μl was used to determine the cellular protein content according to the Lowry method (51) using BSA as a standard. An aliquot of 850 μl of the cell lysate was incubated with 300 μl of HNO_3 (67–70%; BDH ARISTAR PLUS, VWR) at 85 °C overnight followed by 2 h at 95 °C and diluted to 7 ml with MilliQ-water. For the determination of the metal content in media, 10 ml of media were digested with 450 μl of HNO_3. The digested samples and mice tissues were sent for ICP-MS analysis to the Arizona Laboratory for Emerging Contaminants (Tucson, AZ).

Immunocytochemistry and confocal microscopy

CaCo-2 cell monolayers grown on Transwell inserts were washed twice with 2.6 ml (basolateral compartment) and 1.5 ml (apical compartment) of ice-cold $PBS^{Ca/Mg}$ (PBS supplemented with 0.5 mM $MgCl_2$ and 0.9 mM $CaCl_2$, pH 7.2) and subsequently fixed with methanol for 15 min at −20 °C. After adding acetone (prechilled to −20 °C) for 30 s, the cells were washed thrice (5 min each) with $PBS^{Ca/Mg}$. The membranes were excised with a scalpel, transferred to fresh 6-well plates, and blocked with 1% BSA in $PBS^{Ca/Mg}$ for 2 h at room temperature. If not stated otherwise, the cells were washed thrice with $PBS^{Ca/Mg}$ in 5-min intervals between the different steps of the following staining procedure. Incubation of the membranes with rabbit anti–ZO-1 (1:100) and mouse anti–Na^+,K^+-ATPase (1:100) was carried out at 4 °C overnight in humidified atmosphere followed by an incubation with Alexa Fluor 488–conjugated goat anti-rabbit (1:500) and Alexa Fluor 594–conjugated goat anti-mouse antibodies (1:500) in 1% BSA in $PBS^{Ca/Mg}$ for 1 h at room temperature. To visualize the nuclei, the cells were exposed to DAPI (1 $\mu g \times ml^{-1}$ in PBS) for 5 min at room temperature. The membranes were mounted on glass slides with cells facing up in ProLong Diamond antifade mountant (Thermo Fisher Scientific). A coverslip was placed on top of the cells and sealed with nail polish. The images were captured by a Zeiss LSM880 inverted confocal microscope with a 63× oil objective at the Marley Imaging Core of the University of Arizona (Tucson, AZ).

Integrity of the monolayer

Monolayer integrity of CaCo-2 cells was determined by the LY rejection assay. The cells were washed twice with 2.6 ml (basolateral compartment) and 1.5 ml (apical compartment) of $PBS^{Ca/Mg}$, after which the inserts were transferred to fresh 6-well plates. 2.6 ml of prewarmed (37 °C) salt-based incubation buffer (145 mM NaCl, 5.4 mM KCl, 1.8 mM $CaCl_2$, 1 mM $MgCl_2$, 0.8 mM Na_2HPO_4, 50 mM glucose, 20 mM PIPES)

adjusted to pH 7.4 and 1.5 ml of prewarmed (37 °C) incubation buffer containing 12.5 mg × ml^{-1} LY (Sigma–Aldrich) adjusted to pH 6.1 were added to the basolateral and apical compartment, respectively, and the cells were incubated for 4 h at 37 °C in an incubator. An aliquot of 1 ml of incubation buffer was removed from the basolateral compartment every 60 min and replaced by the same volume of fresh incubation buffer adjusted to pH 7.4. At the end of the experiment, the media from both compartments were collected. Standards containing 12.5 μg × ml^{-1} to 6.1 ng × ml^{-1} were prepared in incubation buffer adjusted to pH 7.4. Aliquots of 150 μl of standard or sample were transferred into a well of a black microtiter plate, and fluorescence was quantified using a BioTek Synergy 2 plate reader (BioTek Instruments Inc., Winooski, VT). The pH of the media at the start and the end of the experiment was measured with a Sartorius pHCore pH meter (Sartorius, Lab Instruments GmbH & Co. KG, Goettingen, Germany).

Cell-surface biotinylation

Cell-surface biotinylation was performed on CaCo-2 cell monolayers grown on Transwell inserts. The cells were washed twice with 2.6 ml (basolateral compartment) and 1.5 ml (apical compartment) $PBS^{Ca/Mg}$ prewarmed to 37 °C and twice with $PBS^{Ca/Mg}$ prechilled to 4 °C, after which the insert was transferred to a fresh 6-well plate. For biotinylation of basolateral (apical) surface proteins, 1.5 ml (1 ml) of freshly prepared, ice-cold solution containing 1 mg × ml^{-1} Sulfo-NHS-SS-biotin (Thermo Fisher Scientific) in $PBS^{Ca/Mg}$ was added to the basolateral (apical) compartment, and 1 ml (1.5 ml) of ice-cold $PBS^{Ca/Mg}$ was added to the apical (basolateral) compartment. The cells were incubated on ice in an incubator at 4 °C for 30 min with gentle rocking. The cells were then washed twice with 2.6 ml (basolateral compartment) and 1.5 ml (apical compartment) $PBS^{Ca/Mg}$ prechilled to 4 °C. The reaction was quenched by incubating the cells with 2.6 ml (basolateral compartment) and 1.5 ml (apical compartment) of 100 mM glycine in $PBS^{Ca/Mg}$ for 20 min on ice in an incubator at 4 °C with gentle rocking. Again the cells were washed twice with 2.6 ml (basolateral compartment) and 1.5 ml (apical compartment) of $PBS^{Ca/Mg}$ prechilled to 4 °C. The insert was transferred to a fresh 6-well plate, and the membrane was excised with a scalpel. The cells were lysed in 1 ml of NETT buffer, and the lysate was transferred into 1.5-ml reaction tubes. The lysate was chilled on ice for 20 min with vortexing every 5 min, sonicated with 10 strikes (2 s, amplitude 20) of a Q55 sonicator (Qsonica, Newton, CT) and centrifuged (15,000 × *g*, 4 °C, 15 min). The supernatant was transferred into fresh 1.5-ml reaction tubes. An aliquot of 150 μl (total protein) was frozen in liquid nitrogen and stored at −80 °C for later immunoblot analysis, and 850 μl of the lysates were transferred to Pierce™ centrifuge columns that had been preloaded with 100 μl of Pierce™ high capacity NeutrAvidin™ agarose (both from Thermo Fisher Scientific) according to the manufacturer's protocol. The samples were incubated overnight at 4 °C with slight rocking motion, after which the supernatant was removed by centrifugation for 1 min at room temperature and 1500 × *g*. The agarose beads were washed once with NETT containing protease inhibitor, two times with NETT buffer without protease inhibitor, two times with salt wash buffer (350 mM NaCl, 5 mM EDTA, 0.1% Triton X-100 in PBS, pH 7.4), and three times with NET buffer (150 mM NaCl, 5 mM EDTA, 10 mM Tris, pH 7.4). Between the individual washing steps, the supernatant was removed by centrifugation for 1 min at room temperature and 1500 × *g*. To elute the biotinylated proteins, 100 μl of 1× sample buffer (1.7% (w/v) SDS, 5% (v/v) glycerol, 150 mM DTT, 58 mM Tris, pH 6.8) was added to the agarose beads, and the samples were incubated at 4 °C overnight. On the next day, the centrifuge columns were placed in fresh 1.5-ml reaction tubes, incubated for 30 min at 37 °C, and centrifuged for 2 min at room temperature and 1500 × *g*. The eluate (surface protein) was transferred to fresh 1.5-ml reaction tubes, frozen in liquid nitrogen, and stored at −80 °C for later immunoblot analysis.

Preparation of radiolabeled metal solutions

Radiolabeled metal solutions were prepared on the day of the experiment. 5-Fold concentrated (0.5 μM) radiolabeled manganese solutions were prepared from $^{54}MnCl_2$ (PerkinElmer Life Sciences) complexed to citrate prior to addition to DMEM. 5-Fold concentrated (5 μM) radiolabeled Fe(II) solutions were prepared from $^{59}FeCl_3$ (PerkinElmer Life Sciences) that had been reduced by 5 mM ascorbate prior to addition to DMEM containing 5 mM ascorbate. 5-Fold concentrated (5 μM) radiolabeled Fe(III) solutions were prepared from $^{59}FeCl_3$ that had been complexed to citrate prior to addition to DMEM.

Metal uptake and transport

Metal uptake and transport was studied in CaCo-2 cell monolayers grown on Transwell inserts. During the experiments, the cells were incubated at 37 °C in the humidified atmosphere of an incubator, and all solutions required before the termination of the experiment were prewarmed to 37 °C. At the start of the experiments, the cells were washed twice with 2.6 ml (basolateral compartment) and 1.5 ml (apical compartment) of $PBS^{Ca/Mg}$. The inserts were then transferred to fresh 6-well plates. If not stated otherwise, 2.6 ml of transport medium (DMEM containing 1 mM pyruvate supplemented with 20 mM PIPES) adjusted to pH 7.4 and 1.5 ml of transport medium adjusted to pH 6.1 were added to the basolateral and apical compartment, respectively, and the cells were preincubated for 30 min. Basolateral (apical) metal uptake and basolateral-to-apical (apical-to-basolateral) transport experiments were initiated by replacing 520 μl (300 μl) of transport medium of the basolateral (apical) compartment by the same volume of a freshly prepared 5-fold concentrated radiolabeled metal solution, and the cells were incubated for the desired times. When basolateral-to-apical (apical-to-basolateral) transport was studied an aliquot of 1 ml of medium was removed from the apical (basolateral) compartment for γ-counting by a 2480 WIZARD² Automatic Gamma Counter (PerkinElmer Life Sciences) and replaced by the same volume of the media initially added to the compartment at the time points indicated in the figures. The experiments were stopped by aspirating the media from both compartments and washing the cells three times with ice-cold PBS supplemented with 1 mM EDTA. The cells were lysed in 1 ml of 0.5 M NaOH, and an aliquot of 25 μl was used to determine the cellular protein content according to the

Lowry method (51) using BSA as a standard. An aliquot of 200–800 μl of the lysate were used to quantify the cellular contents of ^{54}Mn and ^{59}Fe by γ-counting.

Statistical analysis

Significance of differences between two sets of data were analyzed using Student's *t* test. Comparisons between multiple sets of data were performed using one- or two-way analysis of variance (ANOVA) followed by the Bonferroni post hoc test: *, $p < 0.05$; **, $p < 0.01$; and ***, $p < 0.001$. $p > 0.05$ was considered as not significant. The PRISM 5 software (GraphPad, La Jolla, CA) was used for statistical analysis.

Author contributions—I. F. S. and N. Z. conceptualization; I. F. S. formal analysis; I. F. S., Y. W., and S. E. M. investigation; I. F. S. visualization; I. F. S., Y. W., S. E. M., and N. Z. methodology; I. F. S. writing-original draft; I. F. S., S. E. M., and N. Z. writing-review and editing; N. Z. resources; N. Z. supervision; N. Z. funding acquisition; N. Z. validation; N. Z. project administration.

Acknowledgments—We thank Dr. Dennis Bernd Nestvogel and Dani Felber for critical reading of the manuscript. We thank Mary Kay Amistadi in the Arizona Laboratory for Emerging Contaminants with the help of ICP-MS measurement. We thank Patty Jansma in the Marley Imaging Core of the University of Arizona for helping us with the acquisition of confocal images.

References

1. Avila, D. S., Puntel, R. L., and Aschner, M. (2013) Manganese in health and disease. *Met. Ions Life Sci.* **13,** 199–227 CrossRef Medline
2. Wedler, F. C. (1994) Biochemical and nutritional role of manganese: an overview. *Health Environ. Res. Online* **FL,** 1–37
3. Weigand, E., Kirchgessner, M., and Helbig, U. (1986) True absorption and endogenous fecal excretion of manganese in relation to its dietary supply in growing rats. *Biol. Trace Elem. Res.* **10,** 265–279 CrossRef Medline
4. Britton, A. A., and Cotzias, G. C. (1966) Dependence of manganese turnover on intake. *Am. J. Physiol.* **211,** 203–206 CrossRef Medline
5. Dorman, D. C., Struve, M. F., James, R. A., McManus, B. E., Marshall, M. W., and Wong, B. A. (2001) Influence of dietary manganese on the pharmacokinetics of inhaled manganese sulfate in male CD rats. *Toxicol. Sci.* **60,** 242–251 CrossRef Medline
6. Davis, C. D., Wolf, T. L., and Greger, J. L. (1992) Varying levels of manganese and iron affect absorption and gut endogenous losses of manganese by rats. *J. Nutr.* **122,** 1300–1308 CrossRef Medline
7. Finley, J. W., Johnson, P. E., and Johnson, L. K. (1994) Sex affects manganese absorption and retention by humans from a diet adequate in manganese. *Am. J. Clin. Nutr.* **60,** 949–955 CrossRef Medline
8. Teeguarden, J. G., Dorman, D. C., Covington, T. R., Clewell, H. J., 3rd, Andersen, M. E. (2007) Pharmacokinetic modeling of manganese: I. Dose dependencies of uptake and elimination. *J. Toxicol. Environ. Health A* **70,** 1493–1504 CrossRef Medline
9. Horning, K. J., Caito, S. W., Tipps, K. G., Bowman, A. B., and Aschner, M. (2015) Manganese is essential for neuronal health. *Annu. Rev. Nutr.* **35,** 71–108 CrossRef Medline
10. Tuschl, K., Meyer, E., Valdivia, L. E., Zhao, N., Dadswell, C., Abdul-Sada, A., Hung, C. Y., Simpson, M. A., Chong, W. K., Jacques, T. S., Woltjer, R. L., Eaton, S., Gregory, A., Sanford, L., Kara, E., *et al.* (2016) Mutations in SLC39A14 disrupt manganese homeostasis and cause childhood-onset parkinsonism-dystonia. *Nat. Commun.* **7,** 11601 CrossRef Medline
11. Boycott, K. M., Beaulieu, C. L., Kernohan, K. D., Gebril, O. H., Mhanni, A., Chudley, A. E., Redl, D., Qin, W., Hampson, S., Küry, S., Tetreault, M., Puffenberger, E. G., Scott, J. N., Bezieau, S., Reis, A., *et al.* (2015) Autosomal-recessive intellectual disability with cerebellar atrophy syndrome caused by mutation of the manganese and zinc transporter gene SLC39A8. *Am. J. Hum. Genet.* **97,** 886–893 CrossRef Medline
12. Park, J. H., Hogrebe, M., Grüneberg, M., DuChesne, I., von der Heiden, A. L., Reunert, J., Schlingmann, K. P., Boycott, K. M., Beaulieu, C. L., Mhanni, A. A., Innes, A. M., Hörtnagel, K., Biskup, S., Gleixner, E. M., Kurlemann, G., *et al.* (2015) SLC39A8 deficiency: a disorder of manganese transport and glycosylation. *Am. J. Hum. Genet.* **97,** 894–903 CrossRef Medline
13. Quadri, M., Federico, A., Zhao, T., Breedveld, G. J., Battisti, C., Delnooz, C., Severijnen, L. A., Di Toro Mammarella, L., Mignarri, A., Monti, L., Sanna, A., Lu, P., Punzo, F., Cossu, G., Willemsen, R., *et al.* (2012) Mutations in SLC30A10 cause parkinsonism and dystonia with hypermanganesemia, polycythemia, and chronic liver disease. *Am. J. Hum. Genet.* **90,** 467–477 CrossRef Medline
14. Tuschl, K., Clayton, P. T., Gospe, S. M., Jr., Gulab, S., Ibrahim, S., Singhi, P., Aulakh, R., Ribeiro, R. T., Barsottini, O. G., Zaki, M. S., Del Rosario, M. L., Dyack, S., Price, V., Rideout, A., Gordon, K., *et al.* (2012) Syndrome of hepatic cirrhosis, dystonia, polycythemia, and hypermanganesemia caused by mutations in SLC30A10, a manganese transporter in man. *Am. J. Hum. Genet.* **90,** 457–466 CrossRef Medline
15. Girijashanker, K., He, L., Soleimani, M., Reed, J. M., Li, H., Liu, Z., Wang, B., Dalton, T. P., and Nebert, D. W. (2008) Slc39a14 gene encodes ZIP14, a metal/bicarbonate symporter: similarities to the ZIP8 transporter. *Mol. Pharmacol.* **73,** 1413–1423 CrossRef Medline
16. Rodan, L. H., Hauptman, M., D'Gama, A. M., Qualls, A. E., Cao, S., Tuschl, K., Al-Jasmi, F., Hertecant, J., Hayflick, S. J., Wessling-Resnick, M., Yang, E. T., Berry, G. T., Gropman, A., Woolf, A. D., and Agrawal, P. B. (2018) Novel founder intronic variant in SLC39A14 in two families causing manganism and potential treatment strategies. *Mol. Genet. Metab.* **124,** 161–167 CrossRef Medline
17. Marti-Sanchez, L., Ortigoza-Escobar, J. D., Darling, A., Villaronga, M., Baide, H., Molero-Luis, M., Batllori, M., Vanegas, M. I., Muchart, J., Aquino, L., Artuch, R., Macaya, A., Kurian, M. A., and Dueñas, P. (2018) Hypermanganesemia due to mutations in SLC39A14: further insights into Mn deposition in the central nervous system. *Orphanet. J. Rare Dis.* **13,** 28 CrossRef Medline
18. Juneja, M., Shamim, U., Joshi, A., Mathur, A., Uppili, B., Sairam, S., Ambawat, S., Dixit, R., and Faruq, M. (2018) A novel mutation in SLC39A14 causing hypermanganesemia associated with infantile onset dystonia. *J. Gene Med.* **20,** e3012 CrossRef Medline
19. Xin, Y., Gao, H., Wang, J., Qiang, Y., Imam, M. U., Li, Y., Wang, J., Zhang, R., Zhang, H., Yu, Y., Wang, H., Luo, H., Shi, C., Xu, Y., Hojyo, S., *et al.* (2017) Manganese transporter Slc39a14 deficiency revealed its key role in maintaining manganese homeostasis in mice. *Cell Discov.* **3,** 17025 CrossRef Medline
20. Liu, C., Hutchens, S., Jursa, T., Shawlot, W., Polishchuk, E. V., Polishchuk, R. S., Dray, B. K., Gore, A. C., Aschner, M., Smith, D. R., and Mukhopadhyay, S. (2017) Hypothyroidism induced by loss of the manganese efflux transporter SLC30A10 may be explained by reduced thyroxine production. *J. Biol. Chem.* **292,** 16605–16615 CrossRef Medline
21. Aydemir, T. B., Kim, M. H., Kim, J., Colon-Perez, L. M., Banan, G., Mareci, T. H., Febo, M., and Cousins, R. J. (2017) Metal transporter Zip14 (Slc39a14) deletion in mice increases manganese deposition and produces neurotoxic signatures and diminished motor activity. *J. Neurosci.* **37,** 5996–6006 CrossRef Medline
22. Jenkitkasemwong, S., Akinyode, A., Paulus, E., Weiskirchen, R., Hojyo, S., Fukada, T., Giraldo, G., Schrier, J., Garcia, A., Janus, C., Giasson, B., and Knutson, M. D. (2018) SLC39A14 deficiency alters manganese homeostasis and excretion resulting in brain manganese accumulation and motor deficits in mice. *Proc. Natl. Acad. Sci. U.S.A.* **115,** E1769–E1778 CrossRef Medline
23. Liuzzi, J. P., Aydemir, F., Nam, H., Knutson, M. D., and Cousins, R. J. (2006) Zip14 (Slc39a14) mediates non-transferrin-bound iron uptake into cells. *Proc. Natl. Acad. Sci. U.S.A.* **103,** 13612–13617 CrossRef Medline
24. Uhlén, M., Fagerberg, L., Hallström, B. M., Lindskog, C., Oksvold, P., Mardinoglu, A., Sivertsson, Å., Kampf, C., Sjöstedt, E., Asplund, A., Olsson, I., Edlund, K., Lundberg, E., Navani, S., Szigyarto, C. A., *et al.* (2015)

Proteomics: tissue-based map of the human proteome. *Science* **347,** 1260419 CrossRef Medline
25. Hubatsch, I., Ragnarsson, E. G., and Artursson, P. (2007) Determination of drug permeability and prediction of drug absorption in Caco-2 monolayers. *Nat. Protoc.* **2,** 2111–2119 CrossRef Medline
26. Sandberg, A. S. (2010) The use of caco-2 cells to estimate fe absorption in humans: a critical appraisal. *Int. J. Vitam. Nutr. Res.* **80,** 307–313 CrossRef Medline
27. Bentz, J., O'Connor, M. P., Bednarczyk, D., Coleman, J., Lee, C., Palm, J., Pak, Y. A., Perloff, E. S., Reyner, E., Balimane, P., Brännström, M., Chu, X., Funk, C., Guo, A., Hanna, I., *et al.* (2013) Variability in P-glycoprotein inhibitory potency (IC_{50}) using various *in vitro* experimental systems: implications for universal digoxin drug–drug interaction risk assessment decision criteria. *Drug Metab. Dispos.* **41,** 1347–1366 CrossRef Medline
28. Gunshin, H., Mackenzie, B., Berger, U. V., Gunshin, Y., Romero, M. F., Boron, W. F., Nussberger, S., Gollan, J. L., and Hediger, M. A. (1997) Cloning and characterization of a mammalian proton-coupled metal-ion transporter. *Nature* **388,** 482–488 CrossRef Medline
29. Tandy, S., Williams, M., Leggett, A., Lopez-Jimenez, M., Dedes, M., Ramesh, B., Srai, S. K., and Sharp, P. (2000) Nramp2 expression is associated with pH-dependent iron uptake across the apical membrane of human intestinal Caco-2 cells. *J. Biol. Chem.* **275,** 1023–1029 CrossRef Medline
30. Hoch, E., and Sekler, I. (2018) Elucidating the H^+ coupled Zn^{2+} transport mechanism of ZIP4: implications in acrodermatitis enteropathica. *bioRxiv* 10.1101/474528 CrossRef
31. Guthrie, G. J., Aydemir, T. B., Troche, C., Martin, A. B., Chang, S. M., and Cousins, R. J. (2015) Influence of ZIP14 (slc39A14) on intestinal zinc processing and barrier function. *Am. J. Physiol. Gastrointest. Liver Physiol.* **308,** G171–G178 CrossRef Medline
32. Rahelic, D., Kujundzic, M., Romic, Z., Brkic, K., and Petrovecki, M. (2006) Serum concentration of zinc, copper, manganese and magnesium in patients with liver cirrhosis. *Coll. Antropol.* **30,** 523–528 Medline
33. Pinilla-Tenas, J. J., Sparkman, B. K., Shawki, A., Illing, A. C., Mitchell, C. J., Zhao, N., Liuzzi, J. P., Cousins, R. J., Knutson, M. D., and Mackenzie, B. (2011) Zip14 is a complex broad-scope metal-ion transporter whose functional properties support roles in the cellular uptake of zinc and nontransferrin-bound iron. *Am. J. Physiol. Cell Physiol.* **301,** C862–C871 CrossRef Medline
34. Zhao, N., Gao, J., Enns, C. A., and Knutson, M. D. (2010) ZRT/IRT-like protein 14 (ZIP14) promotes the cellular assimilation of iron from transferrin. *J. Biol. Chem.* **285,** 32141–32150 CrossRef Medline
35. Canonne-Hergaux, F., Gruenheid, S., Ponka, P., and Gros, P. (1999) Cellular and subcellular localization of the Nramp2 iron transporter in the intestinal brush border and regulation by dietary iron. *Blood* **93,** 4406–4417 Medline
36. Shawki, A., Anthony, S. R., Nose, Y., Engevik, M. A., Niespodzany, E. J., Barrientos, T., Öhrvik, H., Worrell, R. T., Thiele, D. J., and Mackenzie, B. (2015) Intestinal DMT1 is critical for iron absorption in the mouse but is not required for the absorption of copper or manganese. *Am. J. Physiol. Gastrointest. Liver Physiol.* **309,** G635–G647 CrossRef Medline
37. Knöpfel, M., Zhao, L., and Garrick, M. D. (2005) Transport of divalent transition-metal ions is lost in small-intestinal tissue of b/b Belgrade rats. *Biochemistry* **44,** 3454–3465 CrossRef Medline
38. Chua, A. C., and Morgan, E. H. (1997) Manganese metabolism is impaired in the Belgrade laboratory rat. *J. Comp. Physiol. B* **167,** 361–369 CrossRef Medline
39. Geszvain, K., Butterfield, C., Davis, R. E., Madison, A. S., Lee, S. W., Parker, D. L., Soldatova, A., Spiro, T. G., Luther, G. W., and Tebo, B. M. (2012) The molecular biogeochemistry of manganese(II) oxidation. *Biochem. Soc. Trans.* **40,** 1244–1248 CrossRef Medline
40. Missy, P., Lanhers, M. C., Grignon, Y., Joyeux, M., and Burnel, D. (2000) *In vitro* and *in vivo* studies on chelation of manganese. *Hum. Exp. Toxicol.* **19,** 448–456 CrossRef Medline
41. Jayasena, T., Grant, R. S., Keerthisinghe, N., Solaja, I., and Smythe, G. A. (2007) Membrane permeability of redox active metal chelators: an important element in reducing hydroxyl radical induced NAD^+ depletion in neuronal cells. *Neurosci. Res.* **57,** 454–461 CrossRef Medline
42. Bannon, D. I., Abounader, R., Lees, P. S., and Bressler, J. P. (2003) Effect of DMT1 knockdown on iron, cadmium, and lead uptake in Caco-2 cells. *Am. J. Physiol. Cell Physiol.* **284,** C44–C50 CrossRef Medline
43. Hennigar, S. R., and McClung, J. P. (2016) Hepcidin attenuates zinc efflux in Caco-2 cells. *J. Nutr.* **146,** 2167–2173 CrossRef Medline
44. Li, X., Xie, J., Lu, L., Zhang, L., Zhang, L., Zou, Y., Wang, Q., Luo, X., and Li, S. (2013) Kinetics of manganese transport and gene expressions of manganese transport carriers in Caco-2 cell monolayers. *Biometals* **26,** 941–953 CrossRef Medline
45. Leblondel, G., and Allain, P. (1999) Manganese transport by Caco-2 cells. *Biol. Trace Elem. Res.* **67,** 13–28 CrossRef Medline
46. Finley, J. W., and Monroe, P. (1997) Mn absorption: The use of CACO-2 cells as a model of the intestinal epithelia. *J. Nutr. Biochem.* **8,** 92–101 CrossRef
47. Klein, L. D., Breakey, A. A., Scelza, B., Valeggia, C., Jasienska, G., and Hinde, K. (2017) Concentrations of trace elements in human milk: comparisons among women in Argentina, Namibia, Poland, and the United States. *PLoS One* **12,** e0183367 CrossRef Medline
48. Lönnerdal, B., Keen, C. L., Ohtake, M., and Tamura, T. (1983) Iron, zinc, copper, and manganese in infant formulas. *Am. J. Dis. Child.* **137,** 433–437 Medline
49. Ran, F. A., Hsu, P. D., Wright, J., Agarwala, V., Scott, D. A., and Zhang, F. (2013) Genome engineering using the CRISPR-Cas9 system. *Nat. Protoc.* **8,** 2281–2308 CrossRef Medline
50. Cong, L., Ran, F. A., Cox, D., Lin, S., Barretto, R., Habib, N., Hsu, P. D., Wu, X., Jiang, W., Marraffini, L. A., and Zhang, F. (2013) Multiplex genome engineering using CRISPR/Cas systems. *Science* **339,** 819–823 CrossRef Medline
51. Lowry, O. H., Rosebrough, N. J., Farr, A. L., and Randall, R. J. (1951) Protein measurement with the Folin phenol reagent. *J. Biol. Chem.* **193,** 265–275 Medline
52. Taylor, C. A., Hutchens, S., Liu, C., Jursa, T., Shawlot, W., Aschner, M., Smith, D. R., and Mukhopadhyay, S. (2019) SLC30A10 transporter in the digestive system regulates brain manganese under basal conditions while brain SLC30A10 protects against neurotoxicity. *J. Biol. Chem.* **294,** 1860–1876 CrossRef Medline